Supporting Information

A New Family of Decanuclear Ln_7Cr_3 Clusters Exhibiting Magnetocaloric Effect

Jia-Jia Yin,[†a] Tian-Qi Lu,[†a] Cheng Chen,[a] Hai-Yan Shi,[b] Gui-Lin Zhuang,[c] Jun Zheng,[a] Xiaolong Fang[d] and Xiu-Ying Zheng*[a, b]

[a] Institutes of Physical Science and Information Technology, Key Laboratory of Structure and Functional Regulation of Hybrid Materials of Ministry of Education, Photoelectric Conversion Energy Materials and Devices Key Laboratory of Anhui Province, Anhui University, Hefei, 230601, China.

[b] State Key Laboratory of Physical Chemistry of Solid Surfaces and Department of Chemistry, College of Chemistry and Chemical Engineering, Xiamen University, Xiamen, 361005, China.

[c] College of Chemical Engineering, Zhejiang University of Technology, Hangzhou, 310032, China.

[d] College of Materials and Chemical Engineering, Anhui Jianzhu University, Hefei, 230601, China.

E-mail: xyzheng@ahu.edu.cn

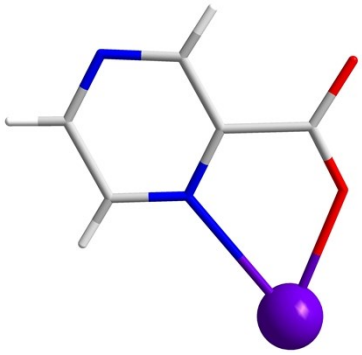

Fig. S1 The bridging mode of the organic ligand L^- in compound **1**.

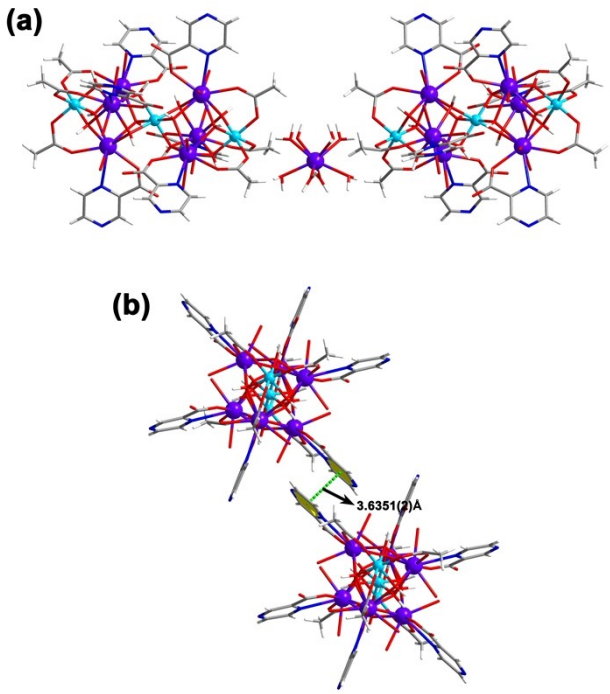

Fig. S2 (a) The hydrogen-bond interaction between the cationic cluster core and the free mononuclear cation of $[Gd(H_2O)_8]^{3+}$; (b) π-bond interactions of the pyrazine groups on the two cationic cluster cores in compound **1**.

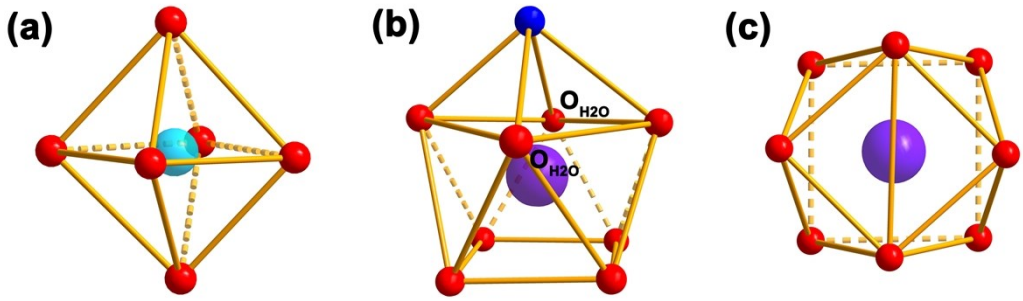

Fig. S3 The coordination modes of Cr^{3+} (a) and Gd^{3+} ions (b, c) in **1**.

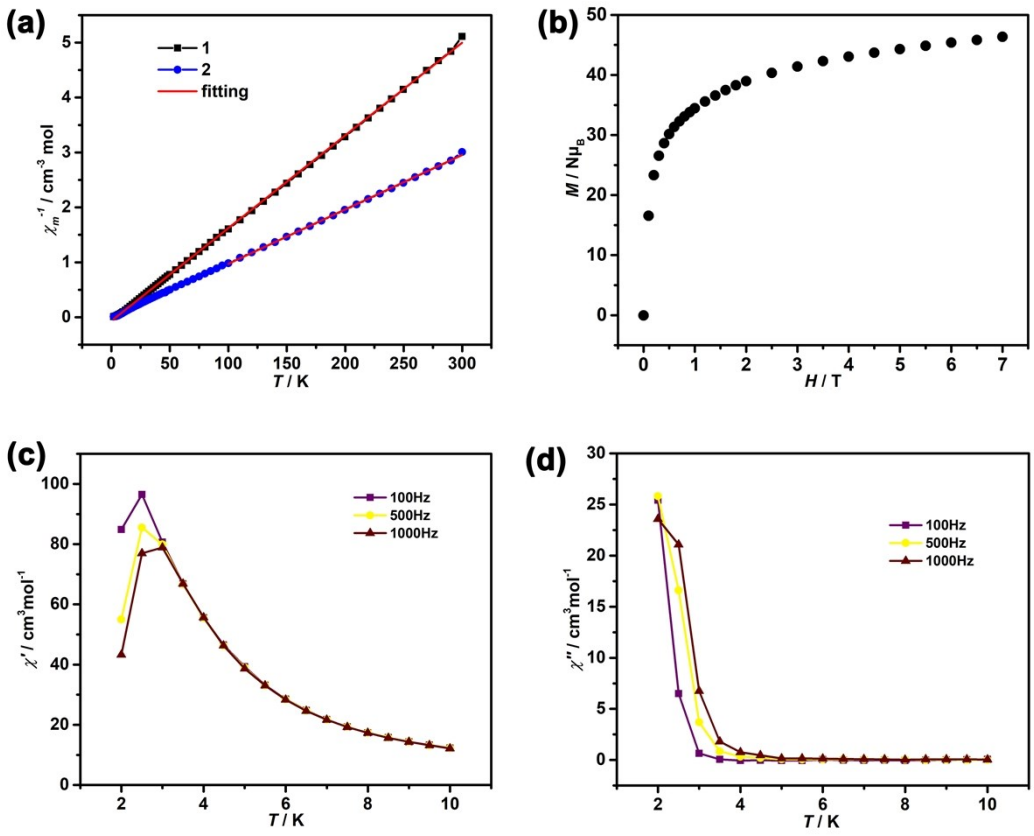

Fig. S4 (a) The $\chi_M T$ *vs* T curves of **1**–**2** were fitted by Curie-Weiss law; (b) the plot of magnetization for **2** at 2 K; (c) temperature dependence of the in-phase and (d) out-of phase ac susceptibilities at the indicated frequencies with H_{dc} = 0 Oe for **2**.

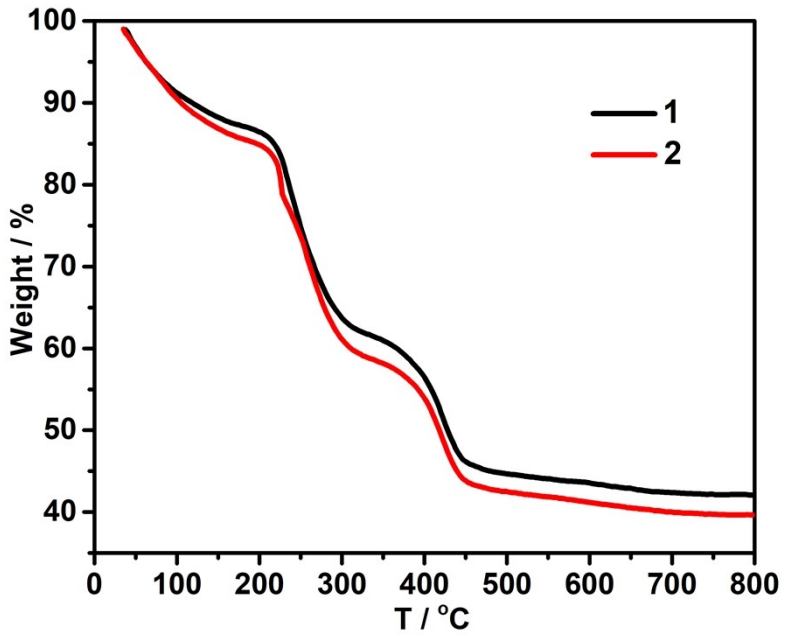

Fig. S5 The TGA of compounds **1**–**2** under air atmosphere.

The TGA of compounds **1**–**2** were measured under air atmosphere. As shown in **Fig. S5**, the mass losses of **1**–**2** at 220 °C are about 15.9 % and 17.1 %, respectively, which are close to the calculated values (15.2 % for **1** and 18.5 % for **2**) for the removal of guest water molecules. As the temperature increase, the metal frameworks of **1**–**2** drastically collapse. The final residues of **1**–**2** (41.8 % and 39.5 %) is slightly higher than the calculated values (36.1 % and 35.2 %) based on Ln_2O_3 (Ln = Gd/Dy) and Cr_2O_3, which may be due to the formation of lanthanide oxychlorides caused by the presence of perchlorates.

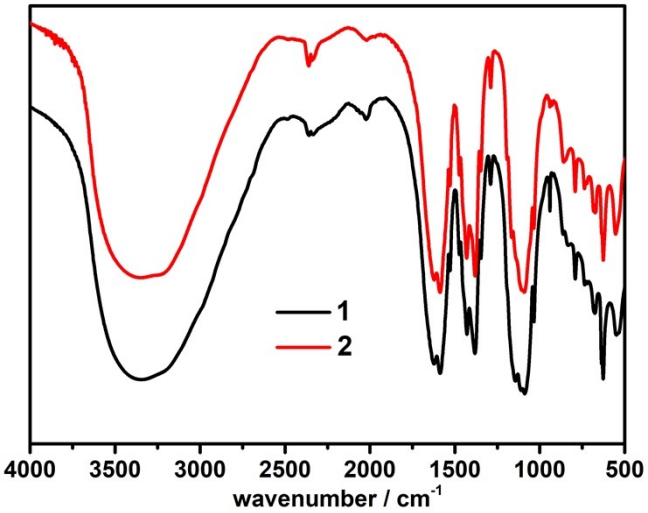

Fig. S6 IR spectra in 500-4000 cm^{-1} for compounds **1**–**2**.

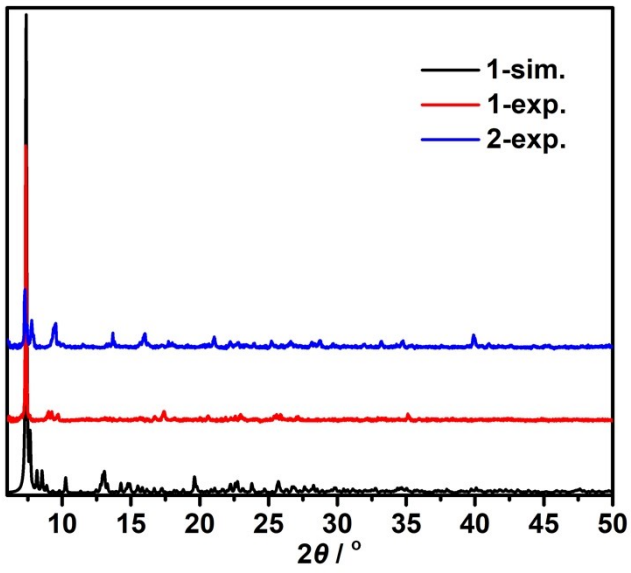

Fig. S7 PXRD curve of compounds **1**–**2**.

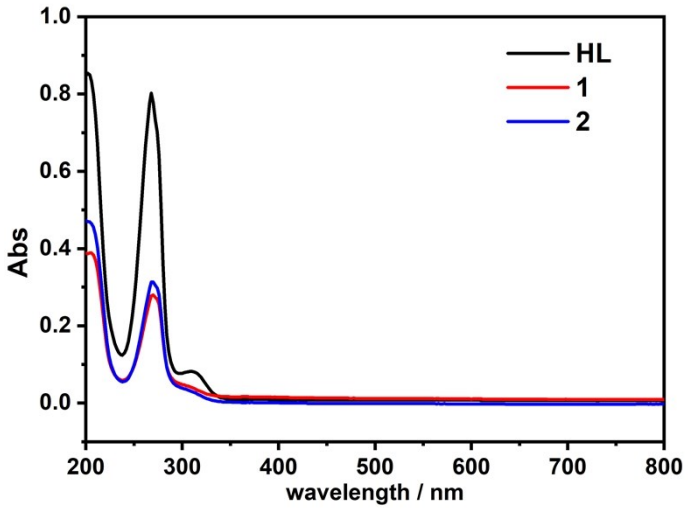

Fig. S8 UV-Vis absorption spectra of HL and compounds **1**–**2**. The result indicates that the main peak at 270 nm belongs to the conjugated transition of the ligand pyrazine ring π–π*.

Table S1. Crystallographic Data for Compounds **1**–**2**.

Compound	**1**	**2**
Formula	$C_{42}H_{158}Cl_6Cr_3Gd_7N_{12}O_{115}$	$C_{42}H_{178}Cl_6Cr_3Dy_7N_{12}O_{125}$
FW	4141.24	4358.15
T/K	120 K	120 K
Cry. system	monoclinic	monoclinic
Space group	*C2/c*	*C2/c*
a /Å	13.9210(14)	13.9146(3)
b /Å	23.943(2)	23.8777(4)
c /Å	41.288(4)	41.1868(8)
α/°	90	90
β/°	96.278(7)	96.592(2)
γ/°	90	90
V /Å^3	13679.0(2)	13593.8(5)
Z	4	4
Dc/g cm^{-3}	2.011	2.129
μ/ mm^{-1}	25.652	24.400
Data/parameters	12189/559	12021/658
2θ/°	7.378–140.032	12.484–138.96
Obs. reflections	25396	24173
F (000)	8144.0	8600.0
GOF	1.129	1.059
$R_1[I> 2\sigma(I)]$[a]	0.0979	0.0649
wR_2(All data)[b]	0.2965	0.1840

[a]$R_1=\sum||F_O| - |F_C||/\sum|F_O|$; [b]$wR_2=\{\sum[w(F_O^2 - F_C^2)^2]/\sum[w(F_O^2)^2]\}^{1/2}$

Table S2. Selected bond distances (Å) and band angles (°) of **1**.

Gd1-O1	2.399(11)	Gd3-O12	2.386(10)
Gd1-O1W	2.389(10)	Gd3-O13[1]	2.460(8)
Gd1-O2W	2.453(10)	Gd3-O15	2.428(8)
Gd1-O8	2.374(10)	Gd3-O16	2.459(9)
Gd1-O14	2.449(8)	Gd3-O18	2.434(9)
Gd1-O15	2.475(8)	Cr1-O13[1]	1.986(8)
Gd1-O16	2.434(8)	Cr1-O13	1.986(8)
Gd2-O3	2.385(11)	Cr1-O14[1]	1.989(8)
Gd2-O3W	2.427(10)	Cr1-O14	1.989(8)
Gd2-O4W	2.438(11)	Cr1-O15	1.981(8)
Gd2-O10	2.337(11)	Cr1-O15[1]	1.981(8)
Gd2-O13[1]	2.441(8)	Cr2-O7	1.978(11)
Gd2-O14	2.469(8)	Cr2-O9	2.013(11)
Gd2-O17	2.429(9)	Cr2-O11	1.959(11)

O1-Gd1-O15	78.3(3)	O5-Gd3-O15	78.3(3)
O1-Gd1-O16	141.6(3)	O5-Gd3-O16	143.0(3)
O1-Gd1-O17	141.6(3)	O5-Gd3-O18	139.5(3)
O1W-Gd1-O1	82.5(3)	O16-Gd3-O13[1]	101.0(3)
O1W-Gd1-O16	135.0(3)	O18-Gd3-O13[1]	67.1(3)
O1W-Gd1-O17	72.2(3)	O13-Cr1-O14[1]	82.4(3)
O2W-Gd1-O15	76.3(3)	O13[1]-Cr1-O14	82.4(3)
O2W-Gd1-O17	136.8(3)	O13[1]-Cr1-O14[1]	97.6(3)
O8-Gd1-O1	130.2(4)	O16-Cr2-O9	177.3(4)
O8-Gd1-O1W	80.5(3)	O17-Cr2-O7	94.4(4)
O3-Gd2-O13[1]	79.7(3)	O17-Cr2-O9	92.6(4)
O3-Gd2-O14	78.4(3)	O7W-Gd4-O7W[2]	131.7(8)
O3W-Gd2-O4W	138.4(4)	O7W-Gd4-O8W[2]	74.4(6)
O3W-Gd2-O13[1]	136.7(3)	O7W-Gd4-O10W[2]	76.7(6)
O3W-Gd2-O14	74.4(3)	O9W-Gd4-O8W	69.7(6)

Symmetry code: [1]1-X,1-Y,1-Z; [2]1-X,+Y,3/2-Z

Table S3. Selected bond distances (Å) and band angles (°) of **2**.

Dy1-O13[1]	2.445(6	Dy3-O16	2.399(6)
Dy1-O15	2.430(6)	Dy3-O17	2.429(7)
Dy1-O16	2.447(6)	Cr1-O13[1]	1.984(6)
Dy2-O3	2.358(7)	Cr1-O13	1.984(6)
Dy2-O3W	2.428(8)	Cr1-O14[1]	1.979(6)
Dy2-O4W	2.417(8)	Cr1-O15[1]	1.982(6)
Dy2-O9	2.377(7)	Cr2-O7	1.983(7)
Dy2-O13[1]	2.431(6)	Cr2-O10	1.995(7)
Dy3-O5	2.356(7)	Cr2-O11	2.009(8)

O1-Dy1-O2W	83.5(3)	O4W-Dy2-O13[1]	136.0(2)
O1-Dy1-O13[1]	77.1(2)	O4W-Dy2-O14	74.2(2)
O1W-Dy1-O18	75.5(2)	O17-Dy2-O13[1]	101.3(2)
O2W-Dy1-O15	73.9(2)	O17-Dy2-O3W	138.5(2)
O8-Dy1-O1W	82.1(3)	O17-Dy2-O14	68.2(2)
O18-Dy1-O14	101.5(2)	O5-Dy3-O17	142.6(2)
O18-Dy1-O15	65.0(2)	O16-Dy3-O14	101.9(2)
O3-Dy2-O3W	80.3(2)	O18-Dy3-O15	68.2(2)
O3-Dy2-O4W	81.4(2)	O18-Dy3-O17	64.9(2)
O3-Dy2-O13[1]	77.4(2)	O14-Cr1-O13	99.0(2)
O3W-Dy2-O14	136.4(2)	O13[1]-Cr1-O13	180.0(2)
O17-Cr2-O11	93.4(3)	O14[1]-Cr1-O13	81.0(2)
O17-Cr2-O16	83.8(3)	O7-Cr2-O10	88.2(3)
O18-Cr2-O9	94.7(3)	O7-Cr2-O11	89.4(3)
O18-Cr2-O11	175.9(3)	O10-Cr2-O11	88.3(3)
O7W[2]-Dy4-O7W	121.1(5)	O7W[2]-Dy4-O8W[2]	74.2(4)
O9W[2]-Dy4-O9W	112.6(6)	O7W-Dy4-O8W[2]	72.9(4)

Symmetry code: [1]1-X,1-Y,1-Z; [2]1-X,+Y,1/2-Z

Table S4. The CShM (Continuous Shape Measures) values of Ln1/Ln4 in compounds **1**–**2**.

Com.[b] / Refcode[a]	**1** Gd1/Gd4	**2** Dy1/Dy4
EP-9	24.061/28.768	23.936/28.205
OPY-9	25.182/24.423	25.417/22.572
HBPY-9	27.906/28.016	28.096/27.636
JTC-9	23.497/25.556	23.375/24.646
JCCU-9	16.864/16.751	16.897/15.557
CCU-9	21.298/17.010	21.362/15.957
JCSAPR-9	**15.376**/22.564	**15.481**/23.486
CSAPR-9	18.633/22.631	18.768/23.844
JTCTPR-9	15.993/**11.047**	16.022/**10.355**
TCTPR-9	20.434/15.644	20.588/14.177
JTDIC-9	25.474/12.705	25.420/12.377
HH-9	23.854/24.677	23.825/23.962
MFF-9	18.061/23.985	18.182/24.540

[a] EP-9, Enneagon; OPY-9, Octagonal pyramid; HBPY-9, Heptagonal bipyramid; JTC-9, Johnson triangular cupola; JCCU-9, Capped cube; CCU-9, Spherical-relaxed capped cube; JCSAPR-9, Capped square antiprism; CSAPR-9, Spherical capped square antiprism; JTCTPR-9, Tricapped trigonal prism; TCTPR-9, Spherical tricapped trigonal prism; JTDIC-9, Tridiminished icosahedron; HH-9, Hula-hoop; MFF-9, Muffin. [b] Two lanthanide ions in each asymmetric unit of **1**–**2.**

The total Hamilton operator of **1** in QMC simulation is presented as follow:

$$H = -\boldsymbol{J_1}*[(S_{Gd1}S_{Gd2} + S_{Gd2}S_{Gd3} + S_{Gd1}S_{Gd3} + S_{Gd4}S_{Gd5} + S_{Gd4}S_{Gd6} + S_{Gd5}S_{Gd6})] - \boldsymbol{J_2}*[(S_{Gd1}S_{Cr1} + S_{Gd2}S_{Cr1} + S_{Gd3}S_{Cr1} + S_{Gd1}S_{Cr2} + S_{Gd2}S_{Cr2} + S_{Gd3}S_{Cr2} + S_{Gd4}S_{Cr2} + S_{Gd5}S_{Cr2} + S_{Gd6}S_{Cr2} + S_{Gd4}S_{Cr3} + S_{Gd5}S_{Cr3} + S_{Gd6}S_{Cr3})] + \boldsymbol{D_1}*[(S_{Z(Gd1)}S_{Z(Gd1)} + S_{Z(Gd2)}S_{Z(Gd2)}) + S_{Z(Gd3)}S_{Z(Gd3)}) + S_{Z(Gd4)}S_{Z(Gd4)}) + S_{Z(Gd5)}S_{Z(Gd5)}) + S_{Z(Gd6)}S_{Z(Gd6)})] + \boldsymbol{D_2}*[(S_{Z(Cr1)}S_{Z(Cr1)} + S_{Z(Cr2)}S_{Z(Cr2)} + S_{Z(Cr3)}S_{Z(Cr3)})]$$